Learned Measurement Correction for Simplified Acoustic Forward Models in Ultrasound Computed Tomography

Luke Lozenski[1,2], Hanchen Wang[3], Brendt Wohlberg[3], Umberto Villa[4], and Youzuo Lin[2]

[1]Department of Electrical and Systems Engineering,
Washington University in St. Louis, St. Louis, MO 63130, USA
[2]Earth and Environmental Sciences Division,
Los Alamos National Laboratory, Los Alamos, NM 87545, USA
[3]Theoretical Division,
Los Alamos National Laboratory, Los Alamos, NM 87545, USA
[4]Oden Institute for Computational Engineering & Sciences,
The University of Texas at Austin, TX, 78712

ABSTRACT

Ultrasound computed tomography (USCT) is an emerging imaging modality that holds great promise for breast imaging. Full-waveform inversion (FWI)-based image reconstruction methods incorporate accurate wave physics to produce high spatial resolution quantitative images of speed of sound or other acoustic properties of breast tissues from USCT measurement data. However, FWI is computationally burdensome and requires a good initial guess of the speed of sound distribution due to the nonconvex nature of the underlying optimization problem (cycle-skipping). Alternatively, the use of a simplified linear model, such as the Born approximation, allows the image reconstruction problem to be formulated as a convex optimization problem, but sacrifices accuracy. This work proposes utilizing a convolutional neural network (CNN) to correct pressure data and accurately reconstruct images using a simplified forward model, thus combining the benefits of accurate reconstructions from traditional FWI methods with the reduced computational complexity of inversion with simplified models. Furthermore, applying this correction to the measurements before inversion avoids issues inherent to other deep learning reconstruction methods that first invert and then apply correction to the images. Specifically, correction in the measurement domain is well-defined by a mathematical model and avoids hallucinations by an improperly learned image prior. This reconstruction approach was validated with a set of anatomically realistic test images and compared to traditional reconstruction methods (FWI and *uncorrected* Born inversion), a data-driven learned reconstruction method, and a machine learning method for artifact correction in the image domain after reconstructing using an inaccurate physics model.

Keywords: Ultrasound computed tomography, Deep learning-based image reconstruction, Physics-informed machine learning, Full waveform inversion, Born approximation, Numerical breast phantom

1. INTRODUCTION

Ultrasound computed tomography (USCT) is an emerging medical imaging technology that can provide high-resolution estimates of tissue acoustic properties, such as speed of sound (SOS), by utilizing ultrasound and tomographic principles.[1] Image formation in USCT is based on the interaction of acoustic wave signals with biological tissues. Quantitative reconstructions of a tissue's acoustic properties from USCT data can then be achieved via a variety of computational methods. Full waveform inversion (FWI)[2,3] is an image reconstruction method that can be utilized to estimate high-resolution maps of acoustic properties from USCT data but requires solving a computationally expensive, nonconvex optimization problem. Alternatively, inversion can be done utilizing a simplified forward model, such as the Born approximation[4] which discards higher order scattering effects, but sacrifices the primary benefit of accuracy.

This work explores multiple model-guided machine learning methods to correct for model mismatch when an estimate of the SOS distribution is reconstructed from USCT data utilizing the Born approximation. These

Further author information: (Send correspondence to Umberto Villa, E-mail: uvilla@austin.utexas.edu, or Youzuo Lin, E-mail: ylin@lanl.gov)

include the application of a convolutional neural network (CNN) for artifact correction in the image domain after reconstruction utilizing an approximate physics model, the proposed CNN approach for data correction in the measurement domain before reconstruction, and the combination of both of these forms of correction for dual correction. These image reconstruction methods utilizing an approximated physics model and assisted by machine learning are also compared to purely data-driven reconstruction methods that learn to create reconstructed images from measurement data.[5,6]

A simulation study was performed to explore these machine learning based reconstruction methods for application in USCT breast imaging. The objects used in this study were a large set of anatomically realistic breast phantoms with stochastically assigned acoustic properties within physiological ranges.[7] Ultrasound measurements were then numerically simulated assuming a stylized 2D ring-array USCT system with 64 sources and 256 receivers and a 96 mm radius. The neural networks used for correction utilized a U-net architecture and were trained on a set of 820 images (214×214 pixels), and tested on an additional 615 images.

2. METHOD

2.1 Wave Equation Model

Assuming a non-lossy medium with homogeneous density and a spatially varying SOS, acoustic propagation in USCT can be modeled using the acoustic wave equation[8]

$$\begin{array}{cc} \frac{1}{c(\mathbf{r})^2}\frac{\partial^2}{\partial t^2}p(\mathbf{r},t) - \Delta p(\mathbf{r},t) = s(\mathbf{r},t) & (\mathbf{r},t) \in \mathbb{R}^d \times (0,T] \\ \frac{\partial}{\partial t}p(\mathbf{r},0) = p(\mathbf{r},0) = 0 & \mathbf{r} \in \mathbb{R}^d, \end{array} \tag{1}$$

where $c = c(\mathbf{r})$ is the spatially varying SOS, $s = s(\mathbf{r},t)$ denotes the excitation pulse, T is the data acquisition time, and $p = p(\mathbf{r},t)$ is the acoustic pressure field. Eqn. (1) defines a well-posed relationship between the SOS c, pressure p and source term s, which can be expressed as $p = \mathcal{H}^c s$.

2.2 Born Model

A simplified model of acoustic wave propagation often used in USCT is based on the Born approximation.[4,9] To derive the Born approximation, the pressure field $p = p_i + p_s$ is decomposed into the isotropic component p_i that satisfies Eqn. (1) for a known constant (or nominal) SOS c_0 and the scattered component p_s. Under the Born model, the approximated scattered component $\tilde{p}_s \approx p_s$ satisfies

$$\begin{array}{cc} \frac{1}{c_0(\mathbf{r})^2}\frac{\partial^2}{\partial t}\tilde{p}_s(\mathbf{r},t) - \Delta\tilde{p}_s(\mathbf{r},t) = \frac{1}{c_0(\mathbf{r})^2}\left(1 - \frac{c_0(\mathbf{r})^2}{c(\mathbf{r})^2}\right)\frac{\partial^2}{\partial t^2}p_i(\mathbf{r},t) & (\mathbf{r},t) \in \mathbb{R}^d \times (0,T] \\ \frac{\partial}{\partial t}\tilde{p}_s(\mathbf{r},0) = \tilde{p}_s(\mathbf{r},0) = 0 & \mathbf{r} \in \mathbb{R}^d. \end{array} \tag{2}$$

Equation (2) defines an affine mapping between $\tilde{p} = p_i + \tilde{p}_s \approx p$ and the squared slowness $b(\mathbf{r}) = \left(\frac{c_0(\mathbf{r})}{c(\mathbf{r})}\right)^2$. In what follows the relationship between $\tilde{p}$ and c under the Born approximation is denoted as $\tilde{p} = \mathcal{H}^c_{\text{Born}} s$.

2.3 Continuous-to-Discrete USCT Imaging Operator

Assuming that J idealized point-like transducers are distributed along the measurement aperture at locations $\mathbf{r}_j \in \mathcal{S}$ $(j = 1, \dots J)$, the sampling operator $\mathcal{M}$ mapping the pressure $p(\mathbf{r},t)$ to the pressure traces matrix $\boldsymbol{g} \in \mathbb{R}^{K\times J}$ is defined as

$$[\mathcal{M}p]_{kj} := [\boldsymbol{g}]_{kj} = p(\mathbf{r}_j, k\Delta T), \quad j = 1, \dots J,\ k = 1, \dots K, \tag{3}$$

where $\Delta T = T/K$ is the sampling interval and K is the number of pressure samples measured over the acquisition interval $[0,T]$. This leads to the continuous-to-discrete imaging relationship

$$\boldsymbol{d}_i = \mathcal{M}\mathcal{H}^c s_i + \boldsymbol{n}_i \approx \mathcal{M}\mathcal{H}^c_{\text{Born}} s_i + \boldsymbol{n}_i \quad i = 1, \dots, I, \tag{4}$$

where $s_i := s_i(\mathbf{r},t)$ is the i^{th} excitation pulse, I is the number of sources, and $\boldsymbol{n}_i \in \mathbb{R}^{K\times J}$ is additive noise.

2.4 Inversion

Inverting for the SOS c given (possibly noisy) measurements $\{\boldsymbol{d}\}_{i=1}^{I}$ can be formulated as one of two optimization problems, the first using the wave equation model

$$\hat{c} := \underset{c}{\operatorname{argmin}} \frac{1}{2} \sum_{i=1}^{I} \|\boldsymbol{d}_i - \mathcal{M}\mathcal{H}^c s_i\|^2 + \mathcal{R}(c) \tag{5}$$

and the second using the Born approximation

$$\hat{c}_{\text{Born}} := \underset{c}{\operatorname{argmin}} \frac{1}{2} \sum_{i=1}^{I} \|\boldsymbol{d}_i - \mathcal{M}\mathcal{H}^c_{\text{Born}} s_i\|^2 + \mathcal{R}(c), \tag{6}$$

where $\mathcal{R}$ is a regularization functional added to incorporate prior information. Solving the first optimization problem, with the accurate model of acoustic propagation $\mathcal{H}^c$ as in Eqn. (5), is known as full-waveform inversion and results in high-resolution reconstructions at the cost of computational complexity. On the other hand, inverting using the Born approximation $\mathcal{H}^c_{\text{Born}}$, as in Eqn. (6), reduces computational complexity and can be framed as a convex penalized linear least-squares optimization problem for the squared slowness b, but comes at the cost of accuracy and resolution due to modeling errors.

2.5 Learned Measurement Correction

This work introduces the use of a convolutional neural network (CNN) as a means of learned measurement correction, or data correction. The network maps data generated using the wave equation model to data generated using the Born approximation. Applying this correction allows for capitalizing on the benefits of both models in inversion, specifically the accuracy of FWI alongside the convexity and computational efficiency of Born inversion.

Applying correction on the measurements before inversion can be viewed as a form of pre-processing and avoids some of the inherent issues of image-to-image deep learning based image reconstruction methods that apply a learned correction in the image domain after inversion (post-processing). First, measurement correction is based on well-posed mathematical relationships as opposed to artifact correction approaches, which are based on learned image priors that cannot be easily defined. Second, the number and size of measurements collected are often much larger than the size of reconstructed images and thus provide richer training sets for learned methods. Third, this method avoids inducing direct bias in the distribution of reconstructed images based on an encoded image prior from training. These three benefits mean that measurement correction is in general an easier map to learn and more generalizable compared to artifact correction in the image domain.

Let $\Psi_\xi : \mathbb{R}^{K\times J} \to \mathbb{R}^{K\times J}$ denote a CNN with weights $\xi \in \mathbb{R}^W$ that maps data generated from the wave equation model to data generated from the Born approximation. This network is trained in a supervised manner by minimizing the data-domain empirical minimum square error loss

$$\min_{\xi} \frac{1}{2} \sum_{n=1}^{N} \sum_{i=1}^{I} \|\boldsymbol{y}_i^n - \Psi_\xi(\boldsymbol{d}_i^n)\|^2 \text{ with } \boldsymbol{d}_i^n := \mathcal{M}\mathcal{H}^{c^n} s_i + \boldsymbol{n}_i^n, \text{ and } \boldsymbol{y}_i^n := \mathcal{M}\mathcal{H}^{c^n}_{\text{Born}} s_i, \tag{7}$$

for a set of training SOS maps $\{c^n\}_{n=1}^N$. Above, $\{\boldsymbol{n}_i^n\}_{n=1,i=1}^{N,I}$ denote *i.i.d.* realizations of measurement noise. Once trained, this network can used to estimate the SOS map $\hat{c}_{DC}$ obtained by solving an optimization problem in the form of Eqn. (6) in which the USCT data $\boldsymbol{d}_i$ are replaced by $\Psi_\xi(\boldsymbol{d}_i)$. That is

$$\hat{c}_{DC} := \underset{c}{\operatorname{argmin}} \frac{1}{2} \sum_{i=1}^{I} \|\Psi_\xi(\boldsymbol{d}_i) - \mathcal{M}\mathcal{H}^c_{\text{Born}} s_i\|^2 + \mathcal{R}(c).$$

3. NUMERICAL STUDY

A simulation study was performed to compare the viability and accuracy of the proposed method for accelerated FWI utilizing machine learning. This study considered six different reconstruction methods applied to the waveform data generated by solving the wave equation model in Eqn. (1). The first method utilized a traditional FWI method, where the exact operator was used for inversion. The second method utilized a large CNN,

Table 1. Numerical study parameters

Virtual USCT System	
Number of sources I	64
Number of receivers M	256
Transducer radius R	96 mm
Number of time samples K	800
Sampling Interval ΔT	0.2 μs
Time horizon T	160 μs
Excitation central frequency f_0	500 kHz
Excitation time shift t_0	3.2 μs
Excitation width σ	10 μs

Image Formation	
Grid size Nx	214
Grid intervals δx	0.6 mm
Training and Testing Sets	
Size of Training Set	820
Size of Testing Set	615
Wave Solver Details	
CFL Number $\frac{c_{max}\delta t}{\delta x}$	0.53
Points per wavelength $\frac{c_{min}}{f_0 \delta x}$	4.7

with the *InversionNet* architecture,[5,6,10] for a data-driven learned reconstruction method. The third method (*Uncorrected*) inverted the waveform data using the Born approximation as imaging operator. The fourth method (*Artifact Corrected*) inverted waveform data using the Born approximation, then utilized a CNN to correct artifacts due to model mismatch.[11] The fifth method(*Data Corrected*), i.e. the the proposed method, utilized a CNN for learned measurement correction before inversion using the Born approximation. The sixth method (*Dual Corrected*) applied the CNN for measurement correction, inverted using the Born approximation, then applied a second CNN for artifact correction.

3.1 Construction of the Speed of Sound Numerical Breast Phantoms

This study made use of anatomically realistic numerical breast phantoms (NBPs) to which spatially varying SOS maps were stochastically assigned within feasible ranges. These NBPs were developed and constructed by Li et al.[7] using tools adapted from the Virtual Imaging Clinical Trial for Regulatory Evaluation (VICTRE) project at the US Food and Drugs Administration[12] for use in USCT virtual imaging studies. Examples of these NBPs are available from.[13] In particular, the generated NBPs are stratified based on the four different levels of breast density.[14] The training set consisted of 820 NBPs while the testing test consisted of 615 NBPs.

3.2 Definition of the Virtual Imaging System and Image Reconstruction Parameters

The measurements geometry consisted of a circular transducer array of radius $R = 96\,\text{mm}$ along which 256 equi-spaced receiving transducers were distributed. Every fourth transducer, 64 in total, also acted as a transmitter. The excitation pulse generated by the i-th emitter was of the form

$$s_i(\mathbf{r}, t) = \delta(\mathbf{r} - \mathbf{r}_i) \exp\left(-\tfrac{(t-t_0)^2}{2\sigma^2}\right) \sin(2\pi f_0 t),\ i = 1, \ldots, I,$$

where $\mathbf{r}_i$ is the location of the i-th emitter, f_0 is the central frequency, $t_0 = 3.2\mu$s is the time shift, and $\sigma = 2\mu$s controls the excitation width. Measurements are collected by firing one transmitter at a time and recording data at every receiver. Waveform data generated by each source are collected over an acquisition time $T = 160\,\mu$s, which is long enough to capture secondary wavefront arrivals. This is repeated for each transmitter and results in multi-channel measurements.

To numerically simulate the pressure field generated by each transmitter, the wave equation in Eqn. (1) and the Born approximation in Eqn. (2) were solved using a finite difference scheme (4th order in space and 2nd order in time) with an absorbing boundary condition using Devito.[15,16] Electronic noise, used to corrupt the FWI data in both reconstruction and training, was modeled as additive white Gaussian noise with a standard deviation of $3.0 \cdot 10^{-5}$, corresponding to an SNR of 20 dB. The imaging system parameters are summarized in Table 1.

3.3 Image Quality Assessment

Image quality was assessed using two methods. The first method was relative root mean square error (RRMSE) defined as

$$\text{RRMSE}(\hat{c}) := \frac{\|c_{true} - \hat{c}\|_2}{\|c_{true} - c_{\text{background}}\|_2}.$$

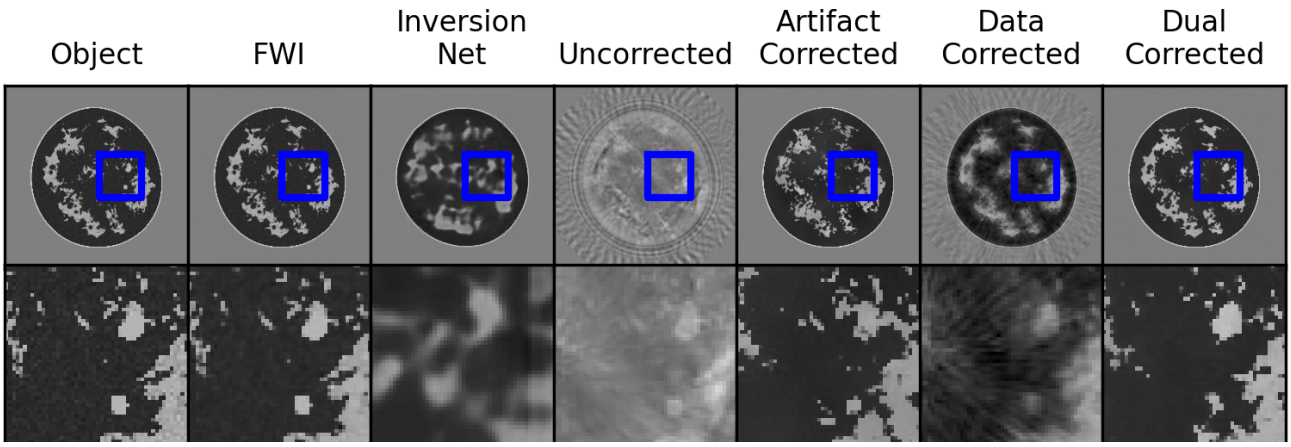

Figure 1. From left to right: True object from the testing set, FWI reconstruction, InversionNet reconstruction, uncorrected Born reconstruction, artifact corrected reconstruction, data correction reconstruction, and dual corrected reconstruction. The bottom row shows a zoomed in feature for each reconstruction, outlined by the blue box. The InversionNet reconstructions and artifact corrected reconstructions look plausible but have false (hallucinated) features. The data corrected reconstruction has improved image quality with minor artifacts from model mismatch. The dual corrected method leads to best image quality among the learned methods.

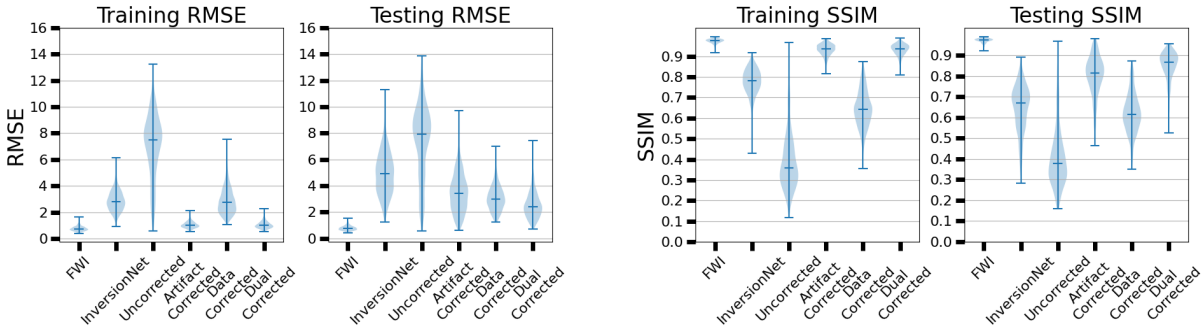

Figure 2. Violin plots of relative root mean square error (RRMSE) and structural similarity index measure (SSIM) obtained by reconstructing images in the training and testing sets using FWI, InversionNet, uncorrected Born approximation and the model-guided learned methods. The *Dual Corrected* method leads to the highest accuracy in terms of RRMSE and SSIM among the learned methods and is comparable to the FWI method.

This method serves as a numerical metric for reconstruction accuracy. The second method was structural similarity index measure (SSIM) as defined in Wang et al.[17] This serves as a metric of perceptual image quality.

4. RESULTS

Reconstructions using each method for a phantom in the testing set are shown in Fig. 1. The FWI reconstruction serves as the reference for image quality. Although plausible, the SOS map estimated by *InversionNet* is highly inaccurate when compared to the true object and contains several hallucinated features. The reconstructed SOS estimate obtained with the *Uncorrected* method is affected by strong artifacts stemming from modeling errors. The *Data Corrected* method is able to remove these artifacts and has a visual appearance similar to the estimate produced by FWI. The *Artifact Corrected* method provides a realistic breast image but introduces hallucinations not present in the true image or in the *Data Corrected* reconstruction. The *Dual Corrected* method does not display any hallucinations and provides higher resolution images than those produced by the *Data Corrected* method.

The RRMSE and SSIM for each reconstruction in the training and testing sets are displayed in Fig. 2 as violin plots. As expected, the *FWI* reconstructions can achieve very low RRMSE and very high SSIM, while the *Uncorrected* reconstructions have the worse performance in terms of both RRMSE and SSIM. The *InversionNet* reconstructions perform worse than the learned methods that leverage the Born approximation in terms of both RRMSE and SSIM on the testing set. The *Data Corrected* method displays better performance on the testing

set than the *Artifact Corrected method*. The *Dual Corrected* method exhibits the highest accuracy in terms of RRMSE and SSIM on the testing set among all learned reconstruction methods.

5. CONCLUSION

This work presents a method for learned measurement correction, or data correction, to enable accurate image reconstruction using a simplified, or approximated, physical model, with application to ultrasound computed tomography (USCT) breast imaging. This data correction method seeks to leverage the structure and richness of physics data to enable ease of training and avoid the inherent bias of similar machine learning approaches for artifact correction in the image domain.

In a computational imaging study, the proposed method of data correction was compared to a physics based full-waveform inversion (FWI) method, a purely data-driven learned reconstruction method that did not incorporate physics, an uncorrected image reconstruction method utilizing the Born approximation, an artifact corrected image reconstruction method, and a method combining both data and artifact correction (dual correction). In this study, reconstruction accuracy was assessed using relative root mean square error (RRMSE) and structural similarity index measure (SSIM). Each form of correction (artifact, data, and dual) greatly improved reconstruction accuracy when compared to the uncorrected Born method and displayed comparable performance to the computationally expensive FWI methods. Comparably, the purely data-driven method lead to inaccurate reconstructions with lower resolution and hallucinated features. This suggests that machine learning methods incorporating an approximated physics model can lead to faster FWI reconstructions while outperforming purely data-driven approaches. Furthermore, in this virtual imaging study, the artifact correction methods showed propensity to introduce hallucinations into reconstructed images that are largely avoided by the data and dual corrected methods. The results of this study suggests that incorporating learned measurement correction helps to avoid the inherent bias in artifact correction and preserves image features.

6. ACKNOWLEDGMENTS

The authors would like to thank Dr. Mark Anastasio and Ph.D. student Fu Li in the Computational Imaging Science Laboratory at the University of Illinois at Urbana-Champaign for providing the numerical breast phantoms used in the numerical studies. This work was funded by the Los Alamos National Laboratory (LANL) - the Center for Space and Earth Science and, in part, by the National Institute of Biomedical Imaging and Bioengineering of the National Institutes of Health under award number R01 EB028652.

REFERENCES

1. N. Duric, P. Littrup, L. Poulo, A. Babkin, R. Pevzner, E. Holsapple, O. Rama, and C. Glide, "Detection of breast cancer with ultrasound tomography: First results with the computed ultrasound risk evaluation (CURE) prototype," *Medical physics* **34**(2), pp. 773–785, 2007.
2. K. Wang, T. Matthews, F. Anis, C. Li, N. Duric, and M. A. Anastasio, "Waveform inversion with source encoding for breast sound speed reconstruction in ultrasound computed tomography," *IEEE transactions on ultrasonics, ferroelectrics, and frequency control* **62**(3), pp. 475–493, 2015.
3. J. Virieux and S. Operto, "An overview of full-waveform inversion in exploration geophysics," *Geophysics* **74**(6), pp. WCC1–WCC26, 2009.
4. R. LeBras and R. W. Clayton, "An iterative inversion of back-scattered acoustic waves," *Geophysics* **53**(4), pp. 501–508, 1988.
5. L. Lozenski, H. Wang, B. Wohlberg, U. Villa, and Y. Lin, "Data driven methods for ultrasound computed tomography," in *Medical Imaging 2023: Physics of Medical Imaging*, **12463**, pp. 141–147, SPIE, 2023.
6. L. Lozenski, H. Wang, F. Li, M. Anastasio, B. Wohlberg, Y. Lin, and U. Villa, "Learned full waveform inversion incorporating task information for ultrasound computed tomography," *IEEE Transactions on Computational Imaging* , 2024.
7. F. Li, U. Villa, S. Park, and M. A. Anastasio, "3-D stochastic numerical breast phantoms for enabling virtual imaging trials of ultrasound computed tomography," *IEEE Transactions on Ultrasonics, Ferroelectrics, and Frequency Control* **69**(1), pp. 135–146, 2022.
8. J. A. Jensen, "A model for the propagation and scattering of ultrasound in tissue," *The Journal of the Acoustical Society of America* **89**(1), pp. 182–190, 1991.

9. A. Stanziola, S. Arridge, B. T. Cox, and B. E. Treeby, "A learned Born series for highly-scattering media," *JASA Express Letters* **3**(5), 2023.
10. Y. Wu and Y. Lin, "Inversionnet: An efficient and accurate data-driven full waveform inversion," *IEEE Transactions on Computational Imaging* **6**, pp. 419–433, 2020.
11. Y. Zhang and H. Yu, "Convolutional neural network based metal artifact reduction in x-ray computed tomography," *IEEE Transactions on Medical Imaging* **37**(6), pp. 1370–1381, 2018.
12. A. Badano, C. G. Graff, A. Badal, D. Sharma, R. Zeng, F. W. Samuelson, S. J. Glick, and K. J. Myers, "Evaluation of digital breast tomosynthesis as replacement of full-field digital mammography using an in silico imaging trial," *JAMA network open* **1**(7), pp. e185474–e185474, 2018.
13. F. Li, U. Villa, S. Park, and M. Anastasio, "2D acoustic numerical breast phantoms and USCT measurement data: V1." Harvard Dataverse, 2021.
14. A. C. of Radiology, C. J. D'Orsi, *et al.*, *ACR BI-RADS Atlas: Breast Imaging Reporting and Data System; Mammography, Ultrasound, Magnetic Resonance Imaging, Follow-up and Outcome Monitoring, Data Dictionary*, ACR, American College of Radiology, 2013.
15. F. Luporini, M. Louboutin, M. Lange, N. Kukreja, P. Witte, J. Hückelheim, C. Yount, P. H. J. Kelly, F. J. Herrmann, and G. J. Gorman, "Architecture and performance of devito, a system for automated stencil computation," *ACM Trans. Math. Softw.* **46**, apr 2020.
16. M. Louboutin, M. Lange, F. Luporini, N. Kukreja, P. A. Witte, F. J. Herrmann, P. Velesko, and G. J. Gorman, "Devito (v3.1.0): an embedded domain-specific language for finite differences and geophysical exploration," *Geoscientific Model Development* **12**(3), pp. 1165–1187, 2019.
17. Z. Wang, A. Bovik, H. Sheikh, and E. Simoncelli, "Image quality assessment: from error visibility to structural similarity," *IEEE Transactions on Image Processing* **13**(4), pp. 600–612, 2004.